Theoretical study on controlling nonlinear behaviors of a coupled-cavity VCSEL by external optical injection

Xiaofeng Li (李孝峰), Wei Pan (潘 炜), Bin Luo (罗 斌), Dong Ma (马 冬), Zheng Zhao (赵 峥), and Guo Deng (邓 果)

School of Computer and Communication Engineering, Southwest Jiaotong University, Chengdu 610031

Received November 19, 2003

A master-slave configuration used to control the nonlinear behaviors arising in a vertical cavity surface emitting laser (VCSEL) with strong external optical feedback is established. In terms of bifurcation diagram, time and frequency domain, the influence of the continuous optical injection from the master VCSEL on the nonlinear characteristics of the slave is investigated theoretically. For relatively weak injection, the slave still keeps its intrinsic nonlinear state. With increasing the injection strength, these nonlinear behaviors evolve to periodic fluctuation, and at last are replaced by the steady-state (e.g. the critical injection parameter for steady-state is 1.2 when external cavity's reflectivity and length are 4% and 4 cm, respectively). During this evolution the bifurcation-contraction phenomena are also observed.

OCIS codes: 130.4310, 250.7260, 140.1540.

In many applications, the semiconductor laser with strong external optical feedback (OFB) generally exhibits complex nonlinear behaviors[1−5]. It is well known that the effect of OFB can, in certain circumstances, be beneficial to narrow the linewidth, enhance the frequency stability[1,6], and tune the working wavelength[7]. But when the OFB level exceeds a critical degree, the laser enters a so-called "coherence collapse" region in which the linewidth is broadened dramatically and the intensity noise is enhanced suddenly[2]. To overcome such unfavorable effects, many possible methods have been proposed, such as the high-frequency injection[3], the appending external cavity technique[8], etc.. Nevertheless, a majority of these studies are in allusion to the edge emitting laser (EEL). It has been shown that vertical cavity surface emitting laser (VCSEL) has the comparable feedback sensitivity to that of the conventional EEL[1,9], and its nonlinear dynamics have been experimentally observed to be similar to those of EEL[1,10−12]. In practical applications of VCSEL, such as optical communication and optical storage, the OFB affects the system performance dramatically, so it is worthy studying how to control these unwanted effects more effectively.

The purpose of this paper is to utilize the external optical injection to control the nonlinear behaviors induced by OFB in VCSEL. Considering the validity of the bifurcation diagram for analyzing the nonlinear dynamic behaviors[13], we study the dependence of them on the injection strength.

A schematic diagram of the chaos control system under consideration is shown in Fig. 1, where $L_{\rm ext}$ is the external cavity length, ISO is the optical isolator, M is the reflector, and BS is the optical beam splitter. This model is based upon the master-slave (M-S) configuration, and the slave (S-VCSEL) is at the chaotic operation with strong OFB. The master (M-VCSEL) provides the continuous wave (CW) output, which is injected into the slave to control the dynamics arising in the slave.

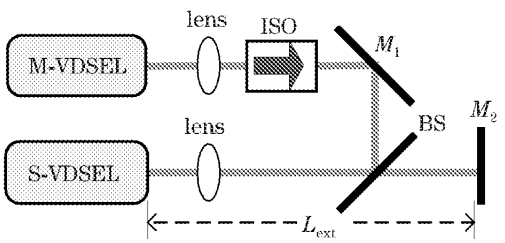

Fig. 1. Schematic diagram of chaos control system by external optical injection.

Generally, the dynamics of the semiconductor lasers are described by the rate equations. To agree with the model accurately, more attentions must be given for two issues: firstly, how to embody the characteristics of VCSEL; secondly, how to modify the traditional rate equations for the M-S configuration. On the one hand, we give the special considerations for the VCSEL's characteristics, which will be discussed later. On the other hand, the corresponding M-S rate equations are established for this M-S model.

Neglecting the spatial dependence of the photon density P, the carrier concentration N, and the injection current density j, we get the following set of rate equations[14]. For the master

$$\frac{{\rm d}P_{\rm m}(t)}{{\rm d}t} = GP_{\rm m}(t) + \beta_{\rm sp}B[N_{\rm m}(t)]^2 - \frac{P_{\rm m}(t)}{\tau_{\rm p}}, \quad (1)$$

$$\frac{{\rm d}N_{\rm m}(t)}{{\rm d}t} = \frac{I}{q\pi w^2 d} - \frac{N_{\rm m}(t)}{\tau_e} - GP_{\rm m}(t), \quad (2)$$

$$\frac{{\rm d}\Phi_{\rm m}(t)}{{\rm d}t} = \frac{1}{2}\beta_c(G - \frac{1}{\tau_{\rm p}}), \quad (3)$$

and for the slave

$$\frac{{\rm d}P_{\rm s}(t)}{{\rm d}t} = GP_{\rm s}(t) + \beta_{\rm sp}B[N_{\rm s}(t)]^2 - \frac{P_{\rm s}(t)}{\tau_{\rm p}} + 2k_{\rm ext}[P_{\rm s}(t)P_{\rm s}(t-\tau)]^{1/2}\cos\theta(t) + 2k_{\rm inj}[P_{\rm s}(t)P_{\rm m}(t-\tau_{\rm inj})]^{1/2}\cos\theta_{\rm inj}(t), \quad (4)$$

$$\frac{{\rm d}N_{\rm s}(t)}{{\rm d}t} = \frac{I}{q\pi w^2 d} - \frac{N_{\rm s}(t)}{\tau_e} - GP_{\rm s}(t), \quad (5)$$

$$\frac{{\rm d}\Phi_{\rm s}(t)}{{\rm d}t} = \frac{1}{2}\beta_c(G - \frac{1}{\tau_{\rm p}}) - k_{\rm ext}[P_{\rm s}(t-\tau)/P_{\rm s}(t)]^{1/2}\sin\theta(t) - k_{\rm inj}[P_{\rm m}(t-\tau_{\rm inj})/P_{\rm s}(t)]^{1/2}\sin\theta_{\rm inj}(t), \quad (6)$$

$$\theta(t) = \omega_0\tau + \Phi_s(t) - \Phi_s(t-\tau), \quad (7)$$

$$\theta_{inj}(t) = \omega_0\tau_{inj} + \Phi_s(t) - \Phi_m(t-\tau_{inj}), \quad (8)$$

where the subscripts 'm' and 's' stand for the M-VCSEL and S-VCSEL, ω_0 is the angular frequency near the threshold. $\tau_p = (V_g\alpha)^{-1}$ is the photon lifetime, where V_g is the group velocity, and $\alpha = \alpha_{int} + \alpha_m$ represents the loss, α_{int} is the intrinsic internal loss and α_m is the cavity mirror loss. w and d are the radius and thickness of the active region, respectively. The detailed parameters and descriptions including those used in the following discussions are listed in Table 1.

The equivalent gain G used in our paper is written as[16]

$$G = \Gamma_z\Gamma_l V_g\alpha_N \frac{\log[N(t)/N_0]}{1+\varepsilon_{NL}P(t)}, \quad (9)$$

where the gain saturation effect is taken into account by introducing the gain suppression factor ε_{NL}. In addition, the usual linear form of gain expression is replaced by a logarithmic one. Although the experiments have verified that the logarithmic form is more appropriate for the special multiple quantum well (MQW) structure of VCSEL, many researchers still use the linear one to study the related problems. The reason is that the linear form is relatively easy to be dealt with. However, in our paper even the logarithmic one can also be managed easily by using the Simulink provided by Matlab. Moreover, in our previous works[13,15], we have used this simulation tool to investigate both the stable and the dynamic behaviors of VCSEL successfully.

The feedback coefficient k_{ext} and injection coefficient k_{inj} are given by[3,17]

$$k_{ext,inj} = \frac{1-R_{eff}}{\tau_{in}}\sqrt{\frac{R_{ext,inj}}{R_{eff}}}, \quad (10)$$

Table 1. Description and Value of VCSEL Parameters[15]

Parameter and Symbol	Value
Lasing Wavelength λ_0	0.85 μm
Longitudinal Confinement Factor Γ_z	1
Lateral Confinement Factor Γ_l	0.07
Group Velocity V_g	8.1×10^9 cm/s
Radius of Active Region w	5 μm
Thickness of Active Region d	0.4 μm
Linewidth Broadening Factor β_c	4.8
Carrier Density at Transparency N_0	1.3×10^{18} cm^{-3}
Spontaneous Emission Factor β_{sp}	1×10^{-4}
Radiative Recombination Rate B	1×10^{-10} cm^3/s
Mirror Reflectivity R_{eff}	0.997
Solitary-Laser Round-Trip Time τ_{in}	0.04 ps
Transmission Delay Time τ_{inj}	66.7 ps
External Round-Trip Time τ	66.7 ps
Equivalent Cavity Loss α	50 cm^{-1}
Gain Suppression Factor ε_{NL}	1×10^{-17} cm^3
Carrier Lifetime at Threshold τ_e	2.7 ns
Gain Coefficient α_N	1.4×10^3 cm^{-1}
Bias Current I	9 mA

where τ_{in} is the solitary-laser round-trip time, R_{eff} is the equivalent reflectivity of the distributed Bragg reflector (DBR), R_{ext} is the external mirror reflectivity. Injection parameter R_{inj} is defined as[17]

$$R_{inj} = \text{Power}_{\text{master\_out}}/\text{Power}_{\text{injecting\_slave}}. \quad (11)$$

Namely, it represents the rate of the master's power injected into the slave laser cavity, and this parameter is a key variable parameter discussed in this paper.

To further exhibit the characteristics of the VCSEL, the following issues must be given special considerations.

Firstly, to solve the problem of low single-pass gain, the DBR with ultrahigh reflectivity is introduced, which leads to two important issues: the equivalent DBR reflectivity R_{eff} and the effective resonant cavity length L_{eff}. Normally, the optical transfer matrix method can be used for the calculation of R_{eff}, e.g., Fig. 2 is the reflection spectrum ($\lambda_0 = 0.98$ μm) resulting from Ref. [18]. To get L_{eff}, the effective length of the top and bottom DBR ($L_{T,B}$) must be ciphered out firstly, and they are given by[19]

$$L_{T,B} = \frac{l_{T,B}}{2}\frac{\tanh[\pi M_{T,B}(n_1^2-n_2^2)/(4n_1n_2)]}{\pi M_{T,B}(n_1^2-n_2^2)/(4n_1n_2)}, \quad (12)$$

$$l_{T,B} = (1/4/n_1 + 1/4/n_2)\lambda_0 M_{T,B}, \quad (13)$$

where the subscribes 'T' and 'B' stand for the top and bottom DBR, respectively, M is the number of pairs, n_1 and n_2 are the refractive indices of the alternating layers, respectively. So the effective cavity length is

$$L_{eff} = L_T + L_B + d + 2L_s, \quad (14)$$

where L_s is the thickness of space layer between DBRs and active region. Moreover there are often two space layers in VCSEL, which are above and beneath of the active region, respectively.

Secondly, the ultrahigh reflectivity of DBR and the short resonant cavity also affect the device behaviors such as the loss, the threshold, as well as the external perturbation sensitivity. The mirror loss is given as

$$\alpha_m = -1/(2L_{eff})\ln(R_T R_B), \quad (15)$$

where R_T and R_B are the equivalent reflectivities of the top and bottom DBR, respectively (in this paper, we choose the same value R_{eff} for them). We can see that

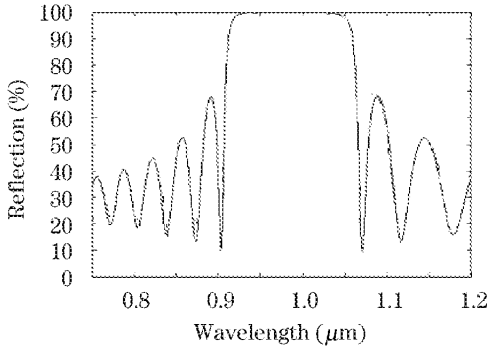

Fig. 2. DBR reflection spectrum.

the larger mirror reflectivity decreases α_m, however, the short cavity lets this parameter vary with contrary direction, which results in a comparable mirror loss as EEL's. For the similar reason, as shown in Ref. [10], VCSEL also has the comparable feedback sensitive to that of EEL.

Thirdly, the small radius and the ultrashort cavity also result in a very small active region volume V, which is one or two numerical degree smaller than that of EEL. In addition, the thickness of the active region equals to the multiplications of the following three parts: the thickness of a single quantum well (SQW), the number of SQW in a block, and the amount of the block in the active region. Allowing for the maximum coupling between the gain region and the optical field, the resonant periodic gain structure is introduced in VCSEL, i.e. the quantum well gain is located at the maximum of the standing wave pattern in the Fabry-Perot (F-P) cavity, which results in a very low threshold.

Finally, the most important characteristic of VCSEL is the micro cavity effect, which not only improves the spontaneous emission rate, but also lets more spontaneous emission couple into the lasing mode (i.e., the spontaneous emission factor is enhanced greatly), which results in an ultra low threshold. Generally, the spontaneous emission factor can be written as[20]

$$\beta_{sp} = 1.5\frac{\Gamma_z K \lambda_0^4}{4\pi^2 n_0^3 V \Delta\lambda}, \tag{16}$$

where K is the Petermann's astigmatism factor, λ_0 is the lasing wavelength, n_0 is the effective index of the cavity, and $\Delta\lambda$ is the full-width at half-maximum (FWHM) of the emission spectrum. We can see from Eq. (16) that a smaller volume and a narrower emission spectrum are beneficial to the increase of the spontaneous emission factor (in ideal condition β_{sp} can be near 1). So in VCSEL, β_{sp} is enhanced with hundreds times, which improves the lasing efficiency greatly.

In a word, to simulate the special device more accurately, the above special means must be taken. In addition, in the M-S system, for a fixed bias current, the dynamics of the considered VCSEL are mainly determined by three factors: R_{ext}, L_{ext} and R_{inj}. Selecting them properly, the VCSEL ought to be controlled in a certain state — the steady state.

The bifurcation diagrams of photon density versus feedback parameter $[F_{ext} = (1 - R_{eff})(R_{ext}/R_{eff})^{1/2}]$ for different injection parameter R_{inj} are shown in Fig. 3, where single density values corresponding to certain F_{ext} represent CW operation, two and more density values denote single-period oscillation and chaos, respectively. We first focused on the no injection case, the result is given in Fig. 3(a). It is obvious that the dynamics of the slave evolves with F_{ext} from CW operation, to single-period, to multi-period, then to chaotic state. Though the laser reenters the single-period region when F_{ext} is between 0.7×10^{-3} and 0.85×10^{-3}, it steps into the chaotic region entirely with the further increasing of the OFB strength.

If there is optical injection in the slave, the dynamics will be affected greatly. Figure 3(b) shows the case of $R_{inj} = 0.06$, and it is seen that even a relatively small amount of injection can affect the dynamics of the

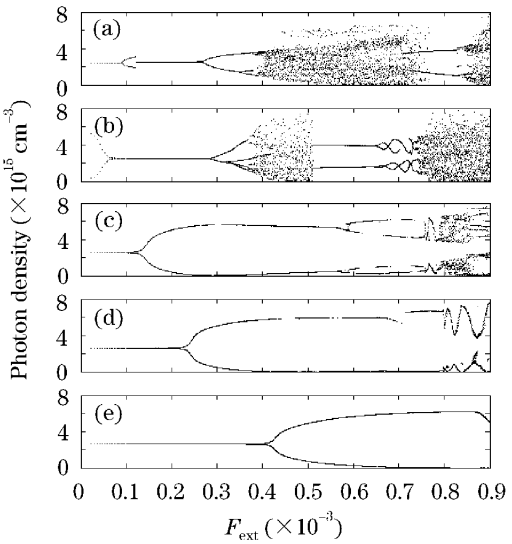

Fig. 3. Bifurcation diagrams of photon density versus feedback strength F_{ext} for various injection parameters R_{inj}. (a) $R_{inj} = 0$; (b) $R_{inj} = 0.06$; (c) $R_{inj} = 0.28$; $R_{inj} = 0.50$; (e) $R_{inj} = 0.80$.

slave dramatically. Comparing with no injection case, the chaos band becomes narrower and the periodic region gets wider remarkably. Moreover, this phenomenon becomes more and more distinct with the further increasing of R_{inj}. Especially, for the case of $R_{inj} = 0.80$ [Fig. 3(e)], the chaotic behaviors of the slave are suppressed completely, and the device merely exhibits CW or single-period behaviors for the range of $F_{ext} \in [0 - 0.9 \times 10^{-3}]$.

To further investigate the effect of the optical injection on the dynamic behaviors of the slave, the time and frequency domains for four chosen values of R_{inj} are plotted in Figs. 4 and 5, where R_{ext} equals 4%. As can be seen from Fig. 4(a) that the slave exhibits chaotic behaviors and outputs randomly for the case of $R_{inj} = 0$, it is also found in the frequency domain [Fig. 5(a)] that there is no dominant frequency component. Figures 4(b) and 5(b) repeat the calculation except that R_{inj} increases to 0.02. It is observed that the slave exhibits single pulse oscillation in the rear half of time domain, and there is not a prime frequency in Fig. 5(b) because the chaos still exists. When $R_{inj} = 0.08$, the behaviors of the slave are seen to change from chaotic to a regular periodic motion. This is shown in Fig. 4(c) together with corresponding frequency domain in Fig. 5(c), which reveals a distinct frequency components corresponding to the OFB induced self-pulse frequency (about 11 GHz). Further increasing R_{inj} up to 1.4, the dynamic behaviors change from periodic motion [Fig. 4(c)] to steady state [Fig. 4(d)]. At this time, the distinct frequency component corresponding to self-pulse decreases dramatically (decreases about eight num- erical degree) and is hardly seen in Fig. 5(d).

In order to investigate in detail how the dynamic behaviors of the slave varying with injection strength, we plot the bifurcation diagram of the photon density versus the injection parameter in Fig. 6, where R_{ext} is 4%. The evolution of the slave's dynamics behaviors with R_{inj} is shown in Table 2 in which the nonlinear state and the

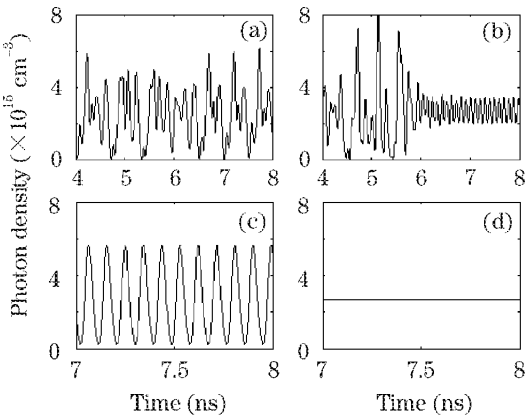

Fig. 4. Temporal variations for different values of $R_{\rm inj}$, where $R_{\rm ext} = 4\%$. (a) $R_{\rm inj} = 0$; (b) $R_{\rm inj} = 0.02$; (c) $R_{\rm inj} = 0.80$; (d) $R_{\rm inj} = 1.40$.

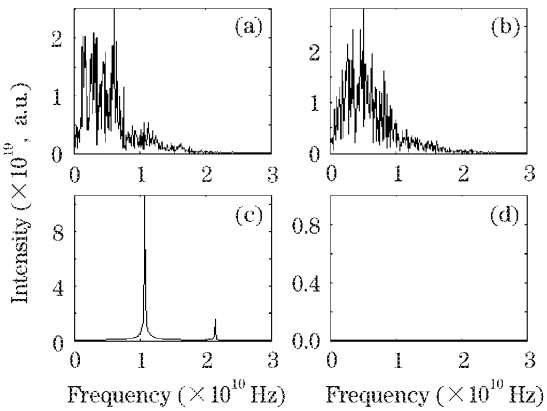

Fig. 5. Frequency domains corresponding to Fig. 4. (a) $R_{\rm inj} = 0$; (b) $R_{\rm inj} = 0.02$; (c) $R_{\rm inj} = 0.80$; (d) $R_{\rm inj} = 1.40$.

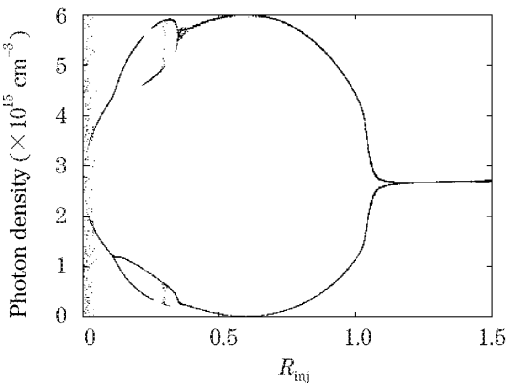

Fig. 6. Bifurcation diagram of photon density versus the injection parameter $R_{\rm inj}$, $R_{\rm ext} = 4\%$.

Table 2. Evolution of Slave's Dynamics with $R_{\rm inj}$

N	State	$R_{\rm inj}$	N	State	$R_{\rm inj}$
1	C	$0 - 0.025$	5	DP	$0.31 - 0.352$
2	SP	$0.025 - 0.15$	6	SP	$0.352 - 1.21$
3	DP	$0.15 - 0.291$	7	S	> 1.21
4	C	$0.291 - 0.31$			

corresponding range of $R_{\rm inj}$ are given. It is clear that when the injection is relatively weak, the slave keeps its own intrinsic nonlinear behaviors. Increasing $R_{\rm inj}$ does not certainly let the slave operate toward the CW state simply, but the double-period and even the chaos can be excited repeatedly. To control the nonlinear behaviors successfully, a very large $R_{\rm inj}$ (> 1.2) is needed, which implies that the injection level must be much larger than the OFB level.

In conclusion, the nonlinear dynamic behaviors induced by OFB in VCSEL can be controlled effectively by the external optical CW injection. Though the optical injection can also induce rich nonlinear behaviors, the nonlinear behaviors can ultimately be replaced by the stable state as long as the injection is strong enough.

This hybrid system can probably be used in the applications where VCSEL acts as the high-speed laser source insensitive to the external optical feedback. In addition, if the strong OFB is introduced in the master to induce the chaotic oscillation, the modified system can also be used to investigate the chaos synchronization, which is a hot topic in recent years due to its application in the secure communication.

This work was supported by the National Natural Science Foundation of China under Grant No. 10174057. X. Li's e-mail address is xf179@163.com.

References

1. Y. C. Chung and Y. H. Lee, IEEE Photon. Technol. Lett. **3,** 597 (1991).
2. L. N. Langley and K. A. Shore, IEE Proceedings: Optoelectronics **144,** 34 (1997).
3. A. T. Ryan, G. P. Agrawal, G. R. Gray, and E. C. Gage, IEEE J. Quantum Electron. **30,** 668 (1994).
4. P. S. Spencer, C. R. Mirasso, and K. A. Shore, IEEE Photon. Technol. Lett. **10,** 191 (1998).
5. M. Houssin, B. Ferrnigier, and M. Desaintfuscien, IEEE J. Quantum Electron. **39,** 833 (2003).
6. K. Hayasaka, Opt. Commun. **206,** 401 (2002).
7. W. Pan, X. X. Zhang, B. Luo, H. C. Lu, and J. G. Chen, Acta Opt. Sin. (in Chinese) **21,** 975 (2001).
8. Y. Liu and J. Ohtsubo, IEEE J. Quantum Electron. **33,** 1163 (1997).
9. K. Petermann, IEEE J. Sel. Top. Quantum Electron. **1,** 480 (1995).
10. A. V. Naumenko and N. A. Loiko, Phys. Rev. A **68,** 033805 (2003).
11. M. Sondermann, H. Bohnet, and T. Ackemann, Phys. Rev. A **67,** 021802 (2003).
12. N. Fujiwara, Y. Takiguchi, and J. Ohtsubo, Opt. Lett. **28,** 896 (2003).
13. G. Deng, W. Pan, and B. Luo, Chin. J. Lasers (in Chinese) **31,** 293 (2004).
14. J. Ohtsubo, IEEE J. Quantum Electron. **38,** 1141 (2002).
15. X. F. Li, W. Pan, B. Luo, G. Deng, and Z. Zhao, Chin. J. Lasers (in Chinese) (to be published).
16. S. F. Yu, W. N. Wong, P. Shum, and E. H. Li, IEEE J. Quantum Electron. **35,** 2139 (1996).
17. A. Murakami, IEEE J. Quantum Electron. **39,** 438 (2003).
18. X. F. Li, W. Pan, B. Luo, G. Deng, and Z. Zhao, Laser Journal (in Chinese) **25,** 6 (2004).
19. F. Koyama, Y. Suematsu, S. Arai, and T. Tawee, IEEE J. Quantum Electron. **19,** 1042 (1983).
20. J. H. Shin, Y. G. Ju, H. E. Shin, and Y. H. Lee, Appl. Phys. Lett. **70,** 2344 (1997).